

Figure suggestions + text fragments for the general discussion:

## 1 Steady-state properties of nongravitating rings

The local steady-state is governed by the balance between the collisional dissipation and the viscous transfer of energy from the systematic orbital motion to random motions. The main source of dissipation comes from the inelasticity of impacts, measured by the  $\epsilon_n$ , the normal coefficient of restitution. In addition, kinetic energy may be lost via frictional forces, reducing the tangential relative velocity between colliding particles; friction also transfers some of the energy of random motions into particles spin motions. In the case of constant  $\epsilon_n$  no energy balance can be achieved if the impacts are too elastic,  $\epsilon_n > \epsilon_{cr}$ , as the dissipation is then too weak to balance the viscous gain of energy due to *local viscosity*, associated to angular momentum flow via particle's radial excursions between impacts; the system inevitably disperses via continuously growing random velocities. The critical  $\epsilon_{cr}$  increases with  $\tau$ , since the reduced mean free path between impacts limits the local viscous gain. Also, allowing for tangential friction,  $\epsilon_t < 1$ , shifts  $\epsilon_{cr}$  closer to unity, as the frictional loss adds to the dissipation due to inelasticity. On the other hand if the constant  $\epsilon_n < \epsilon_{cr}$ , the dissipation exceeds the local viscous gain, leading to reduced eccentricities and inclinations. The eventual steady-state is then determined by the *nonlocal viscous gain* (due to angular momentum transfer across particles in contact), and corresponds to a flattened system where the geometric thickness is of the order of few particle diameters,  $H \sim R$  (in terms of random velocities  $c \sim R\Omega$ ).

However, in the realistic case the coefficient of restitution can be expected to depend on impact velocities. In particular, if  $\epsilon_n$  decreases with impact velocity, a stable steady-state may also be achieved with  $H \gg R$ . The exact value of steady-state velocity dispersion (corresponding to effective  $\epsilon = \epsilon_{cr}$ ) is then determined by the form of the  $\epsilon_n(v_{imp})$  dependence, and at least in principle can range from a thick multilayer of particles to a near monolayer ring. In the latter case the steady-state is in practice indistinguishable from that in the case of constant  $\epsilon_n < \epsilon_{cr}$ . There has been considerable effort put to measuring the coefficient of restitution for icy particles, at the low temperature and pressure appropriate for the planetary ring environment. The extensive laboratory measurements by Bridges et al. (1984) and Hatzes et al. (1988), performed with elaborate pendulum apparatus, have indicated that  $\epsilon_n$  decreases monotonically with  $v_{imp}$ , as required for the thermal balance, and moreover that  $\epsilon_n$  drops to values significantly below unity already for impact velocities of the order of 1 cm/sec. However, the exact form of  $\epsilon_n(v_{imp})$  relation depends sensitively on the surface properties of ice -hardly known for the physical conditions of the rings - as well as on the particle size, via the curvature of the impact point and the effective mass of the impacting bodies.

Fig. ?? shows fits to two laboratory experiments ('frosty' and 'smooth' particles), illustrating the range of uncertainty due to unknown particle properties. In particular, the Bridges et al. (1984)

$$\epsilon_n(v_n) = (v/v_B)^{-0.24} < 1$$

where  $v_B = 0.0077$ cm/sec, has been extensively used in numerical simulations. In Bridges et al.'s experiments the particles had frost on their surfaces, con-

densed during the cooling process of particles. Later measurements reported in Hatzes et al. (1988) had a more accurate control on the surface properties, making it possible to compare smooth frost-free particles, and those with a thin frost layer, or a porous surface. In Fig. ??, their fit ( $v_n$  expressed in cm/sec) to the elasticity of 20cm compacted frost-covered particles is displayed

$$\epsilon_n(v) = 0.90e^{-0.22v_n} + 0.01v_n^{-0.6}$$

In general, for smooth particles the  $\epsilon_n$  values were considerably closer to unity than in Bridges et al.'s original measurement (see Fig.??).

The large uncertainty in the elastic properties of particles reflects directly in the predicted steady-state properties, leading to qualitative differences in the expected stability properties of the system. A system of fairly elastic particles, dynamically hot at low  $\tau$ , exhibits a large reduction of steady-state velocity dispersion as optical depth increases, basically because the local viscous gain becomes less effective as the mean free path between impacts is reduced. In the left panel of Fig.?? this is illustrated in terms of effective geometric thickness: for the model with 'smooth' particles the thickness may drop even by a factor of 5 as  $\tau$  increases from zero to above unity. On the other hand, the dynamically cool 'frosty' particle model has a nearly constant steady state velocity dispersion. This difference in steady-state velocity dispersion reflects in the local and, to a lesser degree, in the non-local contribution to viscosity (right panels). For a cool system the dynamic viscosity, proportional to the product  $\tau\nu$ , is monotonically increasing, because of the dominant role of  $\nu_{nonlocal}$ , whereas for a hot system it becomes a decreasing function for some range of  $\tau$ 's, if the reduction of  $\nu_{local}$  with  $\tau$  is strong enough, due to aforementioned drop in velocity dispersion. A negative  $d(\tau\nu)/d\tau$  should lead to radial instability, whereas a strong enough positive slope may indicate overstability. However, at very large  $\tau$ 's the steady-state properties, including viscosity, are practically independent of elastic model.

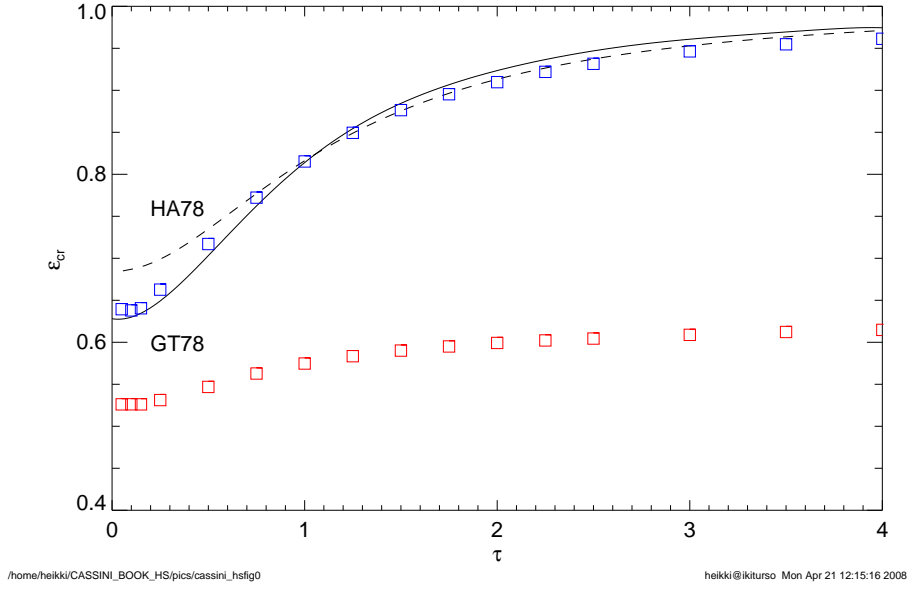
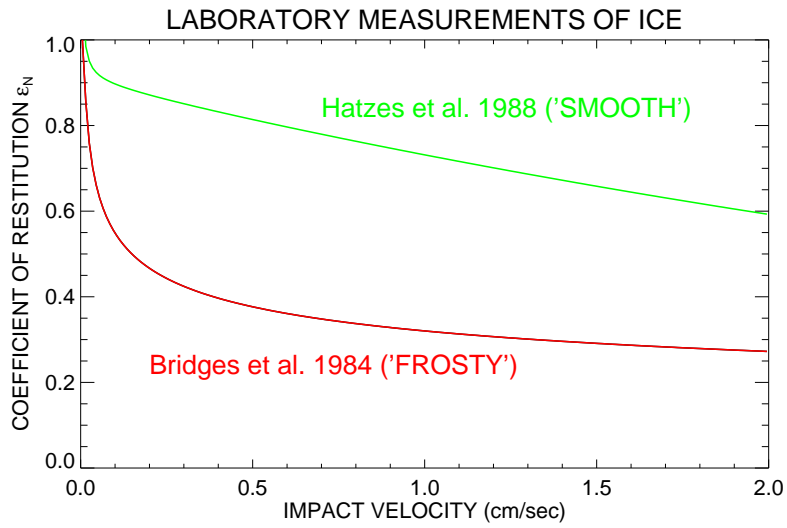


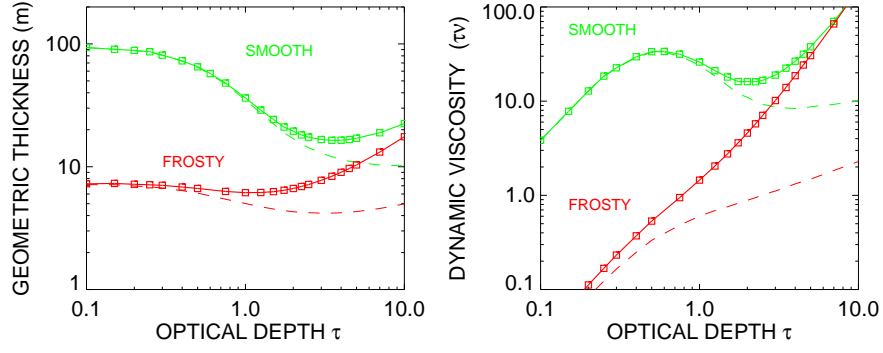
Figure 1: Theoretical thermal stability boundary  $\epsilon_{cr}$  vs.  $\tau$ , according to Hämeen-Anttila (1978) and Goldreich and Tremaine (1978), who used different approximations in the evaluation of collision integrals. For a constant  $\epsilon > \epsilon_{cr}(\tau)$  the viscous dissipation is too weak to balance the viscous gain of energy, leading to rapid dispersal of the ring via increased random velocities. Also shown are the effective steady-state values of  $\epsilon_n$  in two series of simulations, performed with velocity-dependent coefficient of restitution: upper points corresponds to a 'hot' simulation where the velocity dispersion  $c \gg r\Omega$  (this 'mass-point' limit approximates the assumptions behind the theoretical curves), while the lower points correspond to near monolayer simulations performed with the Bridges elasticity formula. The effective  $\epsilon_n$  in simulations is measured by weighting each impact with the square of the normal component of impact velocity,  $\langle \epsilon_n v_n^2 \rangle / \langle v_n^2 \rangle$ . Redrawn from Salo (2001).



/home/heikki/CASSINI\_BOOK\_HS/pics/cassini\_hsfig1\_1

heikki@iki.turku.fi Mon Apr 21 12:21:13 2008

Figure 2: Examples of elastic models applied in simulations. Solid line denotes a fit to laboratory measurements with frosty ice particles (Bridges et al. 1984; 'frosty'), whereas the dashed lines corresponds to measurements where particles had compacted surfaces (Hatzes et al. 1988, 'smooth'). Note that individual measurements had a large scatter around these fitted functions



/home/heikki/CASSINI\_BOOK\_HS/pics/cassini\_hsf1g1\_2

heikki@ikiturso Mon Apr 21 12:21:13 2008

Figure 3: The dependence of steady-state geometric thickness and viscosity on optical depth  $\tau$ , for the two elastic models displayed in Fig. 2. Left frame: symbols show the geometric thickness  $H = \sqrt{12z^2}$  ( $H$  corresponds to the full thickness of a uniform layer with the same dispersion as the actual distribution). Also shown by dotted line is the thickness estimated from the vertical velocity dispersion,  $\sqrt{12}c_z/\Omega$ ; in the case of low filling factor these two measures are identical. However, for flat systems the piling of particles eventually thickens the system although  $c_z$  stays almost constant with  $\tau$ . Right frame: dynamic viscosity  $\tau\nu$ ; the contribution from local viscosity is shown separately with dashed lines. Particle size  $R = 1$  m and Saturnocentric distance  $a = 100\,000$  km are assumed. Note that these plots do not include the effect of selfgravity. Adapted from Salo (2001)

Figure suggestions + text fragments for selfgravity:

## 1.1 Ring self-gravity

Above the local steady-state properties of planetary rings resulting from the balance between the viscous heating and the collisional dissipation of random energy have been discussed. The inclusion of particles' mutual gravitational forces modifies the local dynamics in several, partially competing ways, depending on the density of the ring and the distance from the planet. In low optical depths the collective self-gravity is negligible and the main effect stems from gravitational heating via close binary encounters (Hämeen-Anttila 1984, Ohtsuki XXXX). For larger densities, the mean vertical gravity can become comparable to or even exceed the corresponding component of the central force, implying both a strongly enhanced impact frequency and a reduced ring thickness. However, the ring is then also susceptible to a gravitational instability in planar directions, in practice manifesting as the formation of trailing selfgravity wake structures, *Toomre wakes*. With increased distance from the planet, tidal forces weaken and eventually the direct gravitational sticking of particles becomes possible, causing the particles in wakes to degrade into local aggregates; similar clumping takes place also in low  $\tau$ 's via pairwise sticking of particles. In general, inclusion of selfgravity leads to a strong enhancement of ring viscosity, due to increased impact frequency, and most importantly, due to gravitational torques exerted by the wakes, and by the collective motions associated with them.

A convenient parameter characterizing the importance of selfgravity versus disrupting tidal force is the ratio of the mutual Hill-radius for a pair of identical particles, compared to the sum of their physical radii (e.g. Daisaka et al 2001):

$$r_h = \frac{R_{Hill}}{2r_0}$$

Inserting  $R_{Hill} = (2m_0/3M_{plan})^{1/3}a$ , where  $m_0 = (4\pi\rho/3)r_0^3$  is the mass of the particle,  $r_h$  can be expressed in terms of physical parameters as

$$\begin{aligned} r_h &= \left(\frac{\rho}{12\rho_{plan}}\right)^{1/3} \left(\frac{a}{r_{plan}}\right) \\ &= 0.82 \left(\frac{M_{plan}}{5.69 \cdot 10^{26} \text{ kg}}\right)^{-1/3} \left(\frac{\rho}{900 \text{ kgm}^{-3}}\right)^{1/3} \left(\frac{a}{100\,000 \text{ km}}\right) \end{aligned}$$

where  $r_{plan}$  and  $\rho_{plan}$  denote the radius and density of planet. With these formulas the results for a given  $h_r$  can be scaled to other distances and internal densities of particles. Assuming solid ice density, the main rings of Saturn correspond to  $r_h = 0.6 - 1.1$ , from inner C ring to outer A ring, respectively. Similarly, Uranian rings lay between  $0.65 - 0.8$  if made of ice. Note that instead of  $r_h$  its inverse  $r_p$  is also often employed to parametrize the gravity (e.g. Ohtsuki 1993, Salo 1995); the advantage of using  $r_h$  is that larger values correspond to stronger gravity; also the limit  $r_h = 0$  corresponds to non-gravitating particles.

**Gravitational encounters:** For low  $\tau$  the main effect of gravity comes from close binary encounters, which act like totally elastic impacts: the kinetic energy of the encountering pair is conserved, while the deflection of mutual

orbits transfers energy from the systematic velocity field to random motions. This extra heating is efficient if  $c_x < v_{esc}$ , where  $v_{esc} = \sqrt{2Gm_o/r_o}$  is the mutual escape velocity of particles, but becomes inefficient for  $c_x > v_{esc}$ . Thus, encounters, if acting alone, would establish a state with  $c \sim v_{esc}$  (Cuzzi et al. 1979). However, if the physical impacts are able to maintain  $c > v_{esc}$ , then the effect of encounters is negligible. The condition for the importance of encounters can be written in terms of an upper limit for the vertical thickness,  $H < H_{enc}$ , where the effective thickness defined by  $H = \sqrt{12z^2}$  denotes a full thickness of a uniform layer with the same dispersion as a Gaussian distribution. Since for low optical depths  $\sqrt{z^2} \approx c_z/\Omega$ , and  $c_z/c_x \sim 0.6$ , we have  $H \approx 2c_x/\Omega$ . Writing  $v_{esc} = \sqrt{24r_h^{1.5}r\Omega}$  implies

$$\frac{H}{r_0} \approx 10r_h^{1.5} \quad (1)$$

In the case of constant coefficient of restitution  $\epsilon_n \leq 0.5$ , the impacts alone maintain  $H/r_0 \approx 5$ , which implies that gravitational encounters dominate over physical impacts for  $r_h > 0.7$ .

**Vertical selfgravity:** For larger optical depths the collective effects of self-gravity become increasingly important. First of all, the vertical component of self-gravity,  $F_z$ , may exceed the corresponding component of the central force,  $F_c = -\Omega^2 z$ . For simplicity, assume an infinite homogeneous layer of identical particles with an effective geometric thickness  $H$ . Inside the layer, Poisson equation gives for the vertical selfgravity

$$F_z(z) = -2\pi G \int_{-z}^z \rho(z') dz' = -\frac{4\pi\Sigma z}{H} \quad (2)$$

implying

$$\frac{F_z}{F_c} = \frac{4\pi G\Sigma}{H\Omega^2} = 48\tau r_h^3 \frac{r_o}{H} \quad (3)$$

Including a Gaussian vertical distribution, the vertical self-gravity near the equatorial plane is a factor  $\sqrt{6/\pi}$  larger. Analogous to  $H_{enc}$  we may define  $H_{fz}$  as a thickness of the system for which  $F_z \sim F_c$ ,

$$\frac{H_{fz}}{r_0} \approx 65 \tau r_h^3 \quad (4)$$

For typical values of Saturn's B-ring,  $r_h \sim 0.8$ ,  $\tau \sim 1.5$ , the vertical self-gravity exceeds the central component, unless  $H/r_0 > 50$ . As shown in simulations (Wisdom and Tremaine 1988, Salo 1991) the extra vertical force tends to reduce  $H$  quite markedly, both due to increased vertical frequency itself and also indirectly via the enhanced dissipation (see Fig. 4). This implies a strongly enhanced viscosity for a given  $\tau$ . However, there are other effects of selfgravity which will lead to even more dramatic enhancement of viscosity.

**Gravitational wakes:** Intuitively, the planar components of self-gravity might be expected to have less importance than the vertical component, due to partial cancellation of forces. However, as shown in Toomre (1964), a self-gravitating differentially rotating particle disk would be locally unstable against the growth of axisymmetric disturbances, if its radial velocity dispersion falls below the critical value

$$c_{cr} = \frac{3.36G\Sigma}{\kappa} \quad (5)$$

This critical value offers a very convenient measure for the closeness of the system to the instability threshold: the *Toomre parameter* defined as  $Q = c_x/c_{cr}$ . Writing  $Q$  in terms of the corresponding geometric thickness gives (again assuming identical particles and using relations valid for low  $\tau$ )

$$\frac{H_Q}{r_0} \approx 25Q\tau r_h^3, \quad (6)$$

so that a comparison to Eq. (4) indicates that whenever the vertical selfgravity is important, the system is also near the threshold of collective planar instability:  $F_z/F_c > 1$  corresponds to  $Q < 2$ .

How does this gravitational near-instability manifest? The gravitational collapse is opposed by the particles' random velocities, washing out small scale condensations, and by the differential rotation, dissolving large condensations. As long as  $Q$  exceeds at least a few times unity, the collective instability is completely avoided, and the system remains practically uniform: the main effect of gravity comes via pairwise encounters as described above. However, if the optical depth and thus  $\Sigma$  increases, or if a ring location further away from the planet is inspected,  $Q$  could fall below about 2 – 3. In this case, the collective gravity together with differential rotation leads to the formation of shearing tilted wake structures, with individual wakes forming and dissolving in a time scale  $\sim$  orbital period. The prominence of these structures stems from the swing amplification process (Goldreich and Lynden-Bell 1965, Toomre 1981) which significantly enhances the tiny kinematic wakes triggered by each individual particle. These *Toomre wakes* are analogous to the transient wakes produced by orbiting mass enhancements in a stellar disk (Julian and Toomre 1966, Toomre and Kalnajs 1991), except that in the rings, the dissipation in impacts is able to oppose the gravitational heating induced by the wakes themselves. This allows a statistical steady-state with  $Q \sim 1 - 2$ , characterized with a continuous regeneration of new wakes. Spatial auto-correlation analysis of simulated wakes (Salo 1995, Salo et al. 2004) confirms the close correspondence to Julian-Toomre stellar wakes.

For Saturn's rings, the approximative condition for the formation of wakes,  $Q < 2$  corresponds to (see Salo et al. 2004)

$$\tau > \tau_{min} \approx 0.2 \left( \frac{a}{10^8 \text{m}} \right)^{-3} \left( \frac{\rho}{900 \text{ kg m}^{-3}} \right)^{-1}, \quad (7)$$

or about 0.3 – 0.1, from the inner C ring to the outer A ring, respectively, if the internal density of solid ice is assumed. This gives a conservative *lower* limit, since Eq. 7 is based on the assumption of fairly dissipative identical particles that in the absence of self-gravity would concentrate in a very thin ring, just a few particle diameters thick. This is the expected behavior of particles if they follow the Bridges formula for the coefficient of restitution. In regions with  $\tau > \tau_{min}$ , wakes *may* form, depending on the actual particle elasticity, with more elastic impacts implying an increased  $\tau_{min}$ : see Fig. xx, comparing the 'frosty' and 'smooth' impact models. The formation of wakes is also affected by the particle size distribution: in principle, the presence of large particles provides seeds for strong wakes. This is counteracted, however, by the fact that small particles achieve a larger velocity dispersion than larger particles, which acts as a stabilizing factor. Also, note that  $\tau > \tau_{min}$  is no a strict boundary for the wake formation: weak wakes are always present regardless of  $Q$ .



The average tilt angle of wakes with respect to tangential direction is determined by the gradient of the systematic velocity field, corresponding to about  $20^\circ$  for the Keplerian case; the typical radial spacing between wakes in simulations is close to Toomre's critical wavelength (Toomre 1964)

$$\lambda_{cr} = 4\pi^2 G\Sigma/\kappa^2, \quad (8)$$

where the epicyclic frequency  $\kappa$  equals  $\Omega$  for the Keplerian case. For Saturn's A-ring the expected  $\lambda_{cr} \sim 50 - 100$  meters.

**Gravitational accretion** At large distances gravitational accretion of particles is observed. The condition that the attraction between two radially aligned, synchronously rotating identical particles in contact exceeds the tidal force due to planet is (see e.g. Weidenschilling et al. 1984)

$$(a/r_{plan})^3 > 12(\rho_{plan}/\rho), \quad (9)$$

whereas in the case of two very different sized particles the factor 12 is replaced by 3. In terms of  $r_h$  these conditions correspond to  $r_h > 1$  and  $r_h > 0.79$ ; for icy particles around Saturn this would imply  $a > 126\,000$  and  $80\,000$  km, respectively. However, in actual rings the non-zero velocity dispersion makes accretion more difficult (Ohtsuki 1993, Salo 1992, 1995), and the limiting distances for the formation of aggregates are shifted outward. According to simulations in Karjalainen and Salo (2004), permanent aggregates are able to form for  $r_h > 1.1-1.2$ . The shapes of the forming aggregates are well described with Roche ellipsoids, approaching spherical shapes as the distance increases (Karjalainen and Salo 2004, Porco et al. 2006).

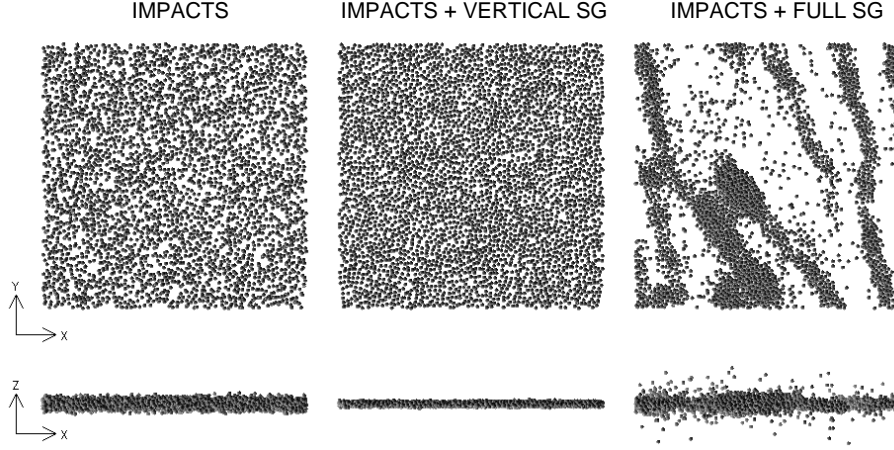


Figure 4: Comparison between vertical and full selfgravity. In the left, only the physical collisions are taking into account, for a simulation system with  $\epsilon_n = 0.5$ ,  $\tau = 0.75$ ,  $r_h = 0.82$  (corresponds to  $a = 100\,000$  km for a solid ice particle density of  $900\text{ kg/m}^3$ , or to  $a = 126\,000$  if  $\rho = 450\text{ kg/m}^3$ ). In the middle, the vertical selfgravity is included, calculated in a self-consistent manner from the vertical density distribution, with the method described in Salo(1991). Near the central plane  $F_z/F_c \approx 8.8$ , corresponding to  $\Omega_z/\Omega = \sqrt{1 + F_z/F_c} \approx 3.1$ : a very similar result would be obtained by the method of Wisdom and Tremaine (1988), who used a constant enhancement factor  $\Omega_z/\Omega = 3.6$  to describe the vertical gravity. In the right, all components of selfgravity are included. In comparison to nongravitating case, the inclusion of vertical gravity reduces the ring thickness from  $H/r_0 = 5.3 \rightarrow 3.3$ , and increases the  $\omega_c$  by about a factor of 8, resulting in two-fold viscosity. However, when full selfgravity is included the viscosity is even 30 times larger than in the nongravitating case. A snapshot from a comoving local simulation region is displayed: x-axis points away from the planet, y axis to the direction of orbital velocity. Note that the size of the simulation system here corresponds to  $2\lambda_{cr} \times 2\lambda_{cr}$ , implying that the wake structure is somewhat suppressed in comparison to what would be obtained with larger calculation regions. From Salo (2001).

BRIDGES-ELASTICITY MODEL

HATZES-ELASTICITY MODEL

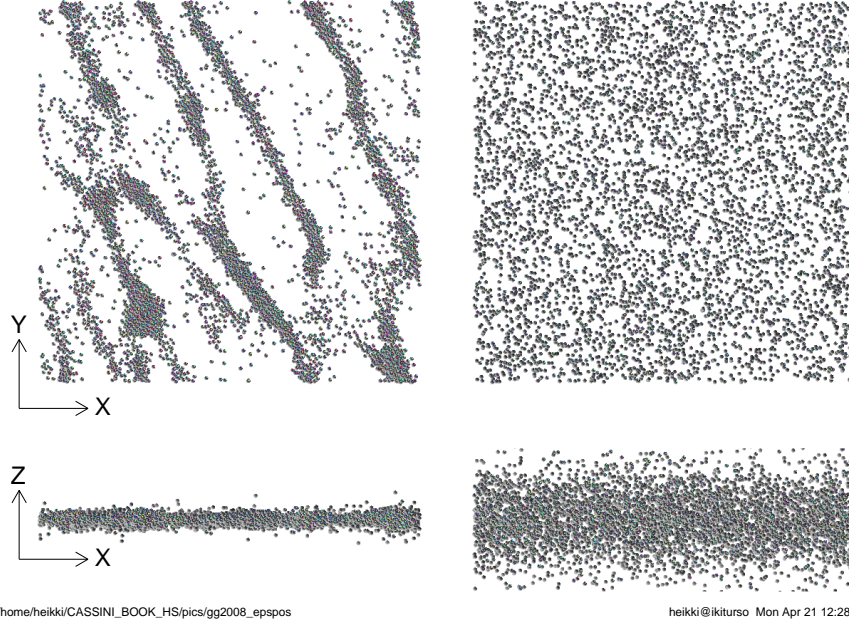


Figure 5: The dependence of simulated selfgravity wakes on the assumed elasticity. In the left Bridges formula 'frosty') is used, while in the right 'smooth' particles are assumed. In the case of elastic particles the influence of self-gravity is strongly reduced. Identical particles with  $\epsilon_n = 0.5$ ,  $\tau = 0.5$  and  $r_h = 0.85$  are simulated, using  $4\lambda_{cr} \times 4\lambda_{cr}$  region. For more details of the effect of elasticity on the wake structure, see Fig. 11 in Salo (1995).

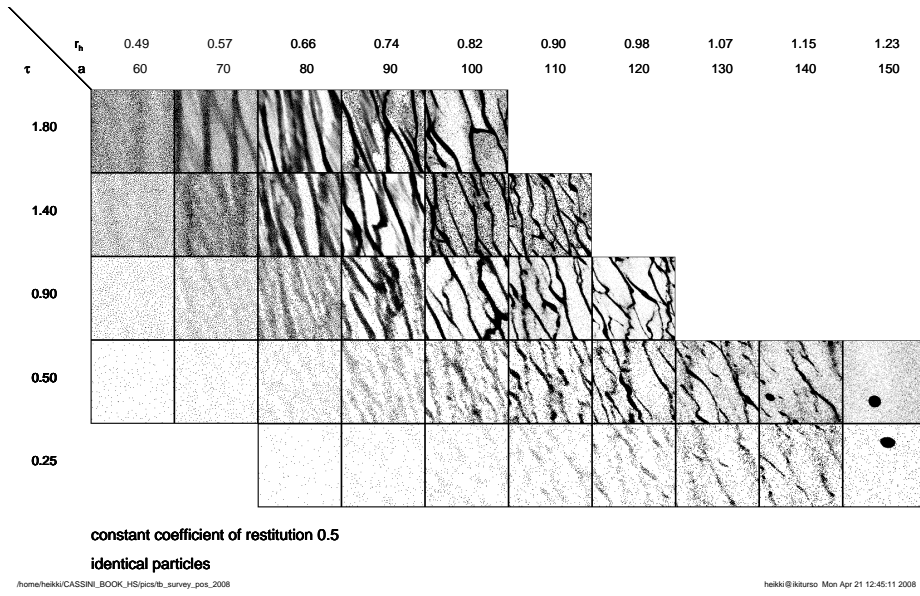
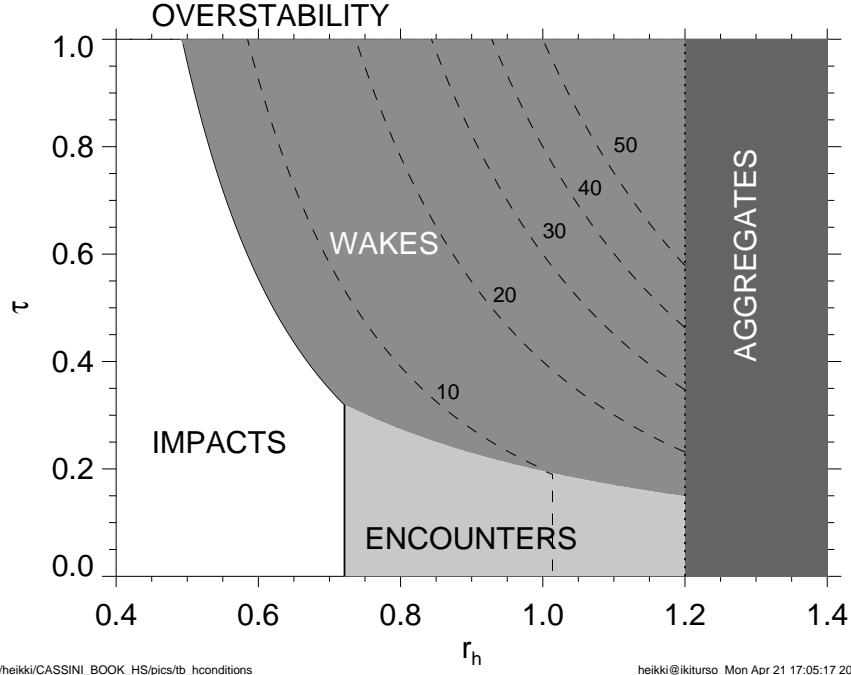


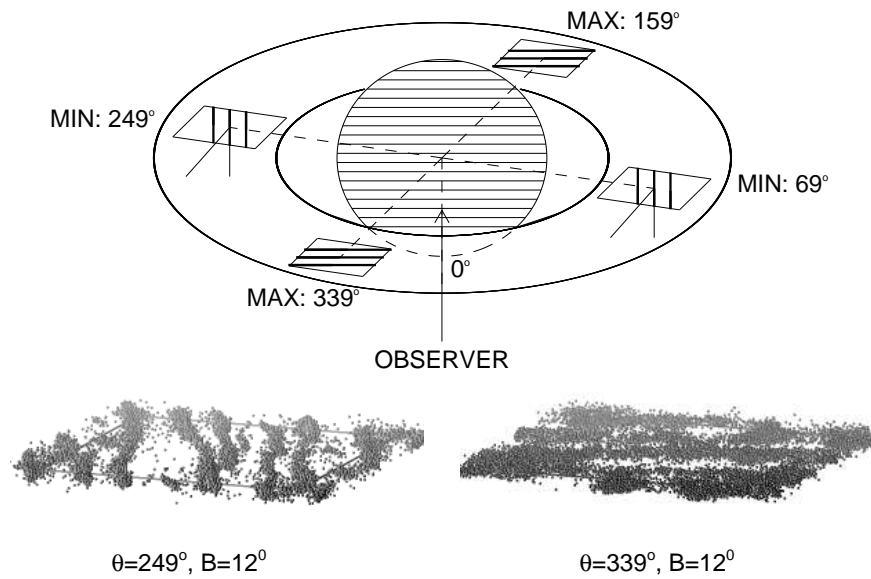
Figure 6: The dependence of selfgravity wakes on the optical depth  $\tau$ , and the strength of gravity vs tidal force, measured by the  $r_h$  parameter. Also indicated are the values of Saturnocentric distance to which  $r_h$  corresponds, in case of solid ice internal density. The size of each region corresponds to  $4\lambda_{cr} \times 4\lambda_{cr}$ . Simulations are performed with the force-method of Salo (1995), and use identical particles with  $\epsilon_n = 0.5$



/home/heikki/CASSINI\_BOOK\_HS/pics/tb\_hconditions

heikki@iikiturso Mon Apr 21 17:05:17 2008

Figure 7: Schematic presentation of the  $(r_h, \tau)$  plane, indicating where different factors govern the local ring dynamics. The boundaries between physical impact-, pairwise gravity- and collective gravity- dominated regions are based on a simple estimate of which ingredient alone would maintain the largest velocity dispersion ( $c_x = 2r\Omega$ ,  $c_x = v_{esc}$ , or  $Q = 2$ , respectively; see the eqs. XX in Salo (1995) and YY in Ohtsuki and Emori (2000)). The contours mark the expected geometric thickness in terms of particle radii. Also indicated is the region of where overstability occurs in simulations, and the boundary beyond which particles clump into local aggregates ( $r_h \approx 1.2$ , see Salo (1995) and Karjalainen and Salo (2004)).



/home/heikki/CASSINI\_BOOK\_HS/pics/asyfig2t\_schema1\_2008

heikki@ikiturso Mon Apr 21 12:50:03 2008

Figure 8: Schematic presentation of wakes and azimuthal brightness asymmetry. From Salo et al (2004).